Noise-sustained structures in differential-flow reactors with autocatalytic kinetics

Bernardo von Haeften* and Gonzalo Izús†
Departamento de Física, Facultad de Ciencias Exactas y Naturales, Universidad Nacional de Mar del Plata, Deán Funes 3350, (7600) Mar del Plata, Argentina
(Received 11 October 2002; published 19 May 2003)

We have studied the formation of noise-sustained structures in a differential-flow reactor with cubic autocatalytic kinetics (the Gray-Scott model). In this system the interplay between advection, diffusion, reaction, and noise fluctuations leads to the formation of noise-sustained patterns in the key species. Numerical integration in one and two spatial dimensions shows that the structures are nonlocally cross correlated. Near threshold, the observed correlation is related to the properties of the convectively unstable critical modes.

DOI: 10.1103/PhysRevE.67.056207 PACS number(s): 89.75.Kd, 05.40.Ca, 47.20.Ky

I. INTRODUCTION

Pattern formation is an ubiquitous manifestation of nonlinearity [1–3] which presents specially interesting features in chemical systems, where the study of spatiotemporal structures supported by reaction-diffusion (RD) systems is actively pursued [2,4]. It is well known that chemical systems that are locally in thermodynamic equilibrium, but held far from the chemical equilibrium, can undergo phase transitions toward new stable states that show striking behaviors. The emerging states may be steady states in which the relative concentrations of the chemical components vary in space (Turing structures) [5], spatially uniform states in which the concentrations of some constituents vary on time (chemical clocks) [6], or even nonlinear traveling waves in the concentrations of some components [7]. A description of many of these phenomena in terms of universal amplitude equations gives the link that relates chemical patterns with those similarly observed in other systems [1,3,8].

A growing interest in mechanisms of pattern formation has been stimulated by the experimental observation of Turing patterns in the chlorite-iodide-malonic acid reaction [9]. As Turing predicted [10], a homogeneous reactive system may lose its stability and develop inhomogeneous structures due to the interaction of diffusion and reaction. In these systems, Turing instability can only take place if there is an autocatalytic species (or activator) and an inhibitor with a diffusion coefficient sufficiently larger than the autocatalytic one, allowing the activator to grow locally while lateral inhibition prevents the spread of growth [11]. However, key species can be disengaged more generally by their differential transport. For example, a homogeneous steady state may be destabilized by flows of activators and inhibitors at different flow rates in the so-called differential-flow-induced chemical instability (DIFICI) mechanism. This instability was predicted [12] and experimentally observed by Menzinger and Rovinsky for the ferroin catalyzed Belousov-Zhabotinsky reaction in a quasi-one-dimensional flow tube [13].

Experimental observation of DIFICI requires a differential-flow reactor. Such a device comprises a flow system in which one or more of the species are immobilized while the remaining species are flowing through the reactor producing an open system. For example, in the so-called packed-bed reactors a solid matrix—usually a cation-exchange resin—is packed inside the reactor and it immobilizes one reactive while the remaining reactants flow and diffuse [13]. An additional cross flow of reagents is applied in cross-flow reactors. This configuration may be achieved, for example, through semipermeable membranes or discrete injection and removal ports positioned along the reactor axis, allowing to keep the system uniformly far from equilibrium [14].

The convective nature of the DIFICI mechanism was recognized in numerical simulations [15] and theoretically established for the Brusselator [16] and the Gray-Scott (GS) kinetics [17,18]. The distinction between absolute and convective instabilities in the unstable region is important to elucidate the mechanisms underlying the formation of dissipative structures; in particular, to separate noise-sustained structures (NSSs) from those originated from the intrinsic dynamics. In the convectively unstable regime, local perturbations of the steady state are advected much rapidly than their rate of spreading [19]. In consequence, the amplitude of a perturbation at a fixed point decays to zero, but it grows in a comoving frame being drifted out of the system in the absence of a continuous source of noise. This is the main difference from the absolutely unstable regime where perturbations grow everywhere in time.

In the GS kinetics the stationary state is globally stable if the flow is below a critical value and it is convectively unstable for all value of flow above threshold [17]. The analogy of the GS system in an open flow configuration with other convectively unstable models suggests that macroscopic NSSs can be expected above the instability threshold [17,19]. In this case, macroscopic patterns can arise and be observed only if noise is continuously applied to regenerate the patterns at any time [23]. When the noise is switched off, the structures disappear through the boundaries and the homogeneous state is recovered. NSSs have been observed in experiments with nematic liquid crystals [20], and they have been also studied in other convectively unstable systems such as Taylor-Couette flows [21,22] and nonlinear optical systems [23,24]. These are examples of a constructive role

*Electronic address: bvhuefte@mdp.edu.ar
†Electronic address: izus@mdp.edu.ar

played by fluctuations in extended dissipative systems. Another example of noise-induced order is the stochastic resonance induced by random modulations on feeding speed in nonlinear chemical reactions [25].

There are convectively unstable systems that exhibit more than one NSS simultaneously. For example, optical parametric oscillators show two locally correlated NSSs at different frequencies or polarization components [24,26–28]. The same situation can also take place in multicomponent convectively unstable chemical systems, where the interplay between diffusion, advection, reaction, and fluctuations can generate NSSs. In this paper we report the existence of NSSs for the DIFICI in the GS model. The NSSs are observed for both key species above the threshold of unstable advection. Numerical simulations indicate that the structures are nonlocally correlated. The correlation, which is expected to depend on the critical modes, is described in terms of a cross-correlation length (CCL).

The paper is organized as follows. Section II reviews the equations for the system. In Sec. III we resume the threshold analysis. The instability is characterized in terms of the eigenfunctions associated with the critical modes. In Sec. IV we study, for one and two spatial dimensions, the generation of NSSs and characterize the typical features of the structures and their correlation. Finally, we summarize the main conclusions in Sec. V.

II. THE MODEL

The GS model that we consider describes a cubic autocatalytic kinetics that takes place in three steps and it is held far from equilibrium by allowing the reaction to advance only in one direction,

$$P \xrightarrow{k_0} A,$$

$$A + 2B \xrightarrow{k_1} 3B,$$

$$B \xrightarrow{k_2} C. \tag{1}$$

A nonequilibrium regime is established by pumping the precursor P at a constant rate and by removing the inert product C as soon as it is produced. The simultaneous presence of A and B enhances the rate of production of B by means of a positive feedback loop in the system. We assume that reactant A is immobilized inside the reactor on a solid support while autocatalyst B is made to flow with a constant velocity v as well as it is able to diffuse with diffusion coefficient D_B. The calculations presented in this paper are carried out for the following dimensionless RD equations:

$$\frac{\partial a}{\partial t} = \mu - ab^2 + \sqrt{\epsilon}\xi(\vec{r},t),$$

$$\frac{\partial b}{\partial t} = \nabla^2 b - \phi\frac{\partial b}{\partial x} - b + ab^2, \tag{2}$$

where $a(\vec{r},t)$ and $b(\vec{r},t)$ are the local concentrations of the chemical species A and B, respectively; and we have introduced the concentration $\sqrt{k_2/k_1}$, time k_2^{-1}, and length $\sqrt{D_B/k_2}$ scales to obtain dimensionless rate equations for A and B [17]. The vector $\vec{r}$ is the spatial vector, t is the time, the Laplacian operator describes diffusion, and the gradient one advection. We remark that the imposed flow breaks the reflection symmetry in the dynamical equations and leads to a convective term (hereafter the advection is taken to occur along the x axis, for simplicity). Dimensionless parameters in Eq. (2) are given by

$$\mu = \frac{k_0 p_0}{k_2}\left(\frac{k_1}{k_2}\right)^{1/2}, \quad \phi = v/\sqrt{k_2 D_B}, \tag{3}$$

where μ measures the constant rate of production of A from P, p_0 is the concentration of P, and ϕ (bifurcation parameter) is a measure of the advection of B. Finally, $\xi(\vec{r},t)$ is a real Gaussian white noise of intensity ϵ, with zero mean and δ-correlated in space and time. This term describes noise for a large variety of practical situations such as thermal noise or input fluctuations as well—for example, in the production of A from P [29,30].

As the reactant A is immobile, boundary conditions (BCs) on this species are not required for the numerical simulations of Eqs. (2). Dirichlet BC is assumed at the inlet of the reaction domain ($x=0$) and Neumann BC at the end of the reactor ($x=L_X$). The length L_X is choosen in such a way that any spatiotemporal pattern that evolves does so well before it reaches the right end of the reactor. For two-dimensional (2D) reactors, Neumann BC are assumed for the y coordinate ($0 \leqslant y \leqslant L_Y$).

III. LINEAR INSTABILITY ANALYSIS

A. Threshold analysis

In this section we briefly recall the linear stability analysis of the steady state solution of Eqs. (2) corresponding to the chemical reactor operating below the DIFICI threshold. The uniform steady state is

$$a_0 = \mu^{-1}, \quad b_0 = \mu. \tag{4}$$

The eigenvalues $\omega_{1,2}(\vec{q})$ of the linear instability problem are obtained in terms of the wave vectors $\vec{q}=(q_x,q_y)$ through the following dispersion relation [17]:

$$\omega^2 + \omega(q^2 + \mu^2 - 1 + iq_x\phi) + \mu^2(q^2 + 1 + iq_x\phi) = 0, \tag{5}$$

where $q^2 = q_x^2 + q_y^2$ (one-dimensional case, $q_x = q$). By increasing ϕ the homogeneous symmetric solution becomes unstable at $\phi = \phi_c$, where $\phi_c = \phi(\vec{q}_c)$ is the minimum on the neutral curve

$$\phi^2 = \frac{(1+q^2)(1-q^2-\mu^2)^2}{q_x^2(1-q^2)}. \tag{6}$$

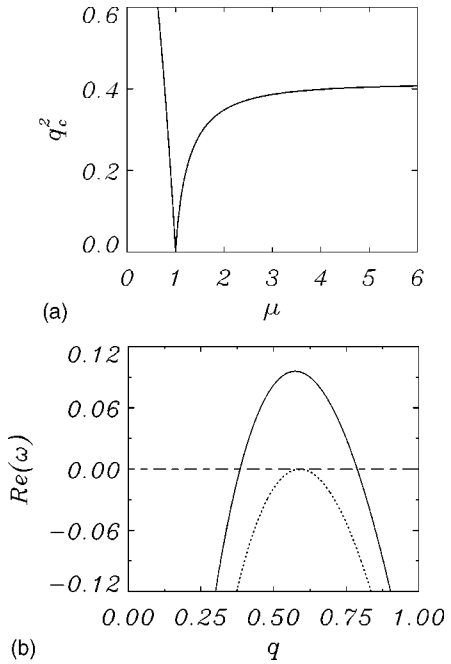

FIG. 1. (a) Critical wave number as a function of μ. (b) Real part of the eigenvalue ω as a function of q. The solid line corresponds to $\phi=9.5$ and the dotted line corresponds to criticality. Here $\mu=2$ ($\phi_c=8.1605$, $q_c=0.5899$). The most unstable modes correspond to the maximum of each line. The level $\mathrm{Re}(\omega_c)=0$ is also indicated as a dashed horizontal line as reference.

The critical unstable modes are traveling waves $a,b \sim \exp(i\vec{q}_c\cdot\vec{r}+i\Omega_c t)$ with wave vector $\vec{q}_c=(\pm q_c,0)$ and frequency of oscillation,

$$\Omega_c = Im(\omega_c) = \pm q_c \frac{\mu^2\phi_c}{1-q_c^2-\mu^2}. \tag{7}$$

In Ref. [17] it was shown that the instability is convective for all $\phi \geqslant \phi_c$, and the threshold for Eqs. (2) does not depend on the BCs, except for periodic BCs, which are not considered here [17].

The instability threshold ϕ_c depends on μ. For $\mu<1$, the convective instability takes place at zero advection ($\phi_c=0$), while for $\mu>1$ the threshold increases monotonically with μ. In particular, $\phi_c \sim 2\sqrt{2}(\mu-1)^{1/2}+\cdots$ for $\mu\to 1^+$ and $\phi_c \sim (1+\sqrt{2})\mu^2$ for $\mu \gg 1$. In all the cases the instability takes place at a finite wave vector except for $\mu=1$, where the critical mode is the homogeneous one [see Fig. 1(a)]. For $\phi>\phi_c$, there is a band of unstable modes. To illustrate this point, in Fig. 1(b) we show the real part of the critical eigenvalue ω_c as a function of q for the critical case $\phi=\phi_c$ and for one case above threshold. All the modes with $\mathrm{Re}(\omega)>0$ are linearly unstable.

B. Critical modes

Next we consider some features of the early time dynamics that can be understood in terms of the eigenvectors corresponding to the eigenvalues of the linearized problem discussed above. In Fig. 2 we show numerical results, in the presence of noise, for typical profiles of $a(x+\Delta x,t)$ and $b(x,t)$ after ϕ is increased beyond its threshold value. The results correspond to snapshots for a short time in a one-dimensional (1D) case. The selected value of Δx—which will be introduced below—reveals that species A and B support nonlocally cross-correlated NSSs. To quantify this phenomenon, the following cross-correlation function $C(t,z)$ at equal times is introduced:

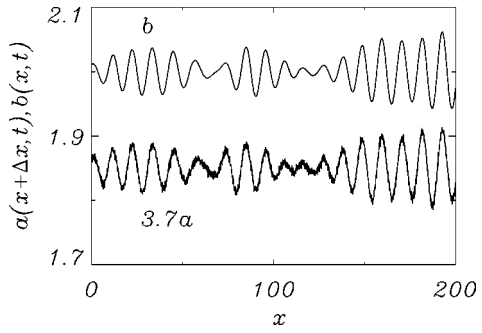

FIG. 2. a and b as functions of x for $t=8$ (short time). Note that a is shifted in $\Delta x=3.6$ and it is magnified by a scale factor 3.7 to obtain an appreciable curve. Parameter values are $\mu=2.0$, $\phi=9.5$, $\epsilon=5\times10^{-8}$, and $L_X=800$.

$$\begin{aligned} C(t,z) &= C\{a(x,t),b(x,t),z\} \\ &= \int [a(x+z,t)-\langle a\rangle][b(x,t)-\langle b\rangle]dx/\sqrt{\sigma(a)\sigma(b)}, \end{aligned} \tag{8}$$

where $\langle\cdot\rangle$ denotes the mean value in space and $\sigma(\cdot)$ is the corresponding variance. In Fig. 3(a) we show $C(t,z)$ as a function of z for a short time: A maximum of order 1 is observed at $z=\Delta x$ reflecting the high nonlocal cross correlation between the NSSs. This correlation persists on time, as we show in Fig. 3(b) where the time evolution of $C(t,\Delta x)$ is showed for a typical realization of Eqs. (2). Note that for a short time the structures are not well developed (they have small amplitude) but they are highly correlated. In consequence, after a transition time, uncorrelated initial conditions evolve toward correlated NSSs characterized by a CCL.

These numerical facts can be explained in terms of the eigenvectors associated with the critical eigenvalue ω_c introduced in Eq. (5). At threshold, the eigenvectors $\Lambda(\vec{q},x)$ are damped for any $\vec{q}$ except for $\vec{q}_c=\pm q_c\hat{x}$, which are marginal (zero growth rate) and define the direction in the functional space along which the convective instability takes place:

$$\begin{aligned} \begin{bmatrix} a-a_0 \\ b-b_0 \end{bmatrix} &\sim \Lambda_{\pm}(q_c,x)\exp(\pm i\Omega_c t) \\ &= \kappa(\mu,q_c)\begin{bmatrix} \sqrt{4/(\mu^4+\Omega_c^2)}\exp(\pm iq_c\Delta x) \\ 1 \end{bmatrix} \\ &\quad\times\exp(\pm iq_c x)\exp(\pm i\Omega_c t), \end{aligned} \tag{9}$$

where the amplitude

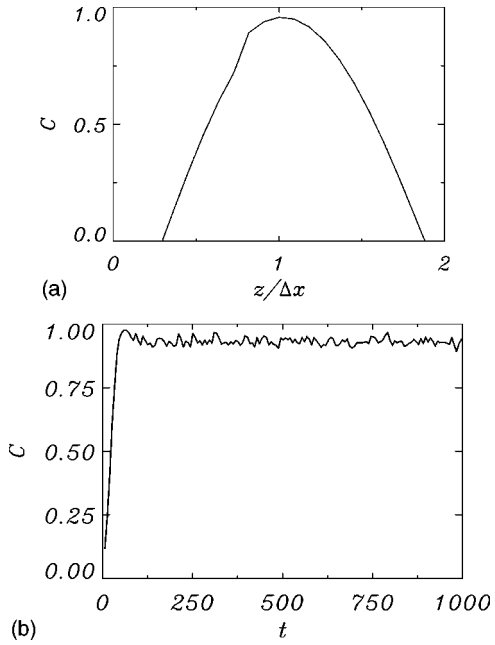

FIG. 3. (a) $C(t,z)$ as a function of $z/\Delta x$ for the NSSs shown in Fig. 2. (b) Cross correlation $C(t,\Delta x)$ as a function of time for a characteristic realization of Eqs. (2). The value of the parameters are the same of Fig. 2.

$$\kappa^{-1}(\mu,q_c)=2\pi\sqrt{1+\frac{2}{\mu^4(1-q_c^2)}} \tag{10}$$

is a normalization factor and Δx is the CCL introduced before, given at threshold by

$$\Delta x=\frac{\lambda_c}{2}\left(1-\frac{1}{\pi}\arcsin\sqrt{\frac{1+q_c^2}{2}}\right), \tag{11}$$

where λ_c is the critical wavelength. In Fig. 4 we show that Δx is a monotonically decreasing function of μ.

The form of the critical eigenvectors explains our numerical finding that at short times, when the linear approximation to the dynamics remains valid, species A and B sustain patterns with the same wave vector but they are nonlocally cross correlated in space. Although Δx is not defined at threshold

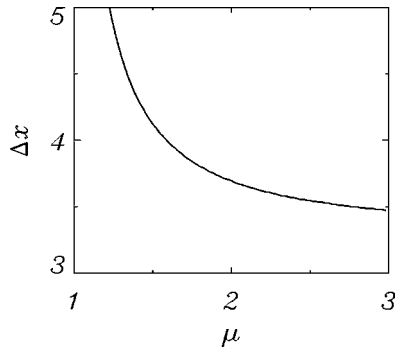

FIG. 4. Δx as a function of μ. Note that along the curve, ϕ_c varies $[\phi_c=\phi_c(\mu)]$, in particular $\phi_c\to 0$ for $\mu\to 1^+$.

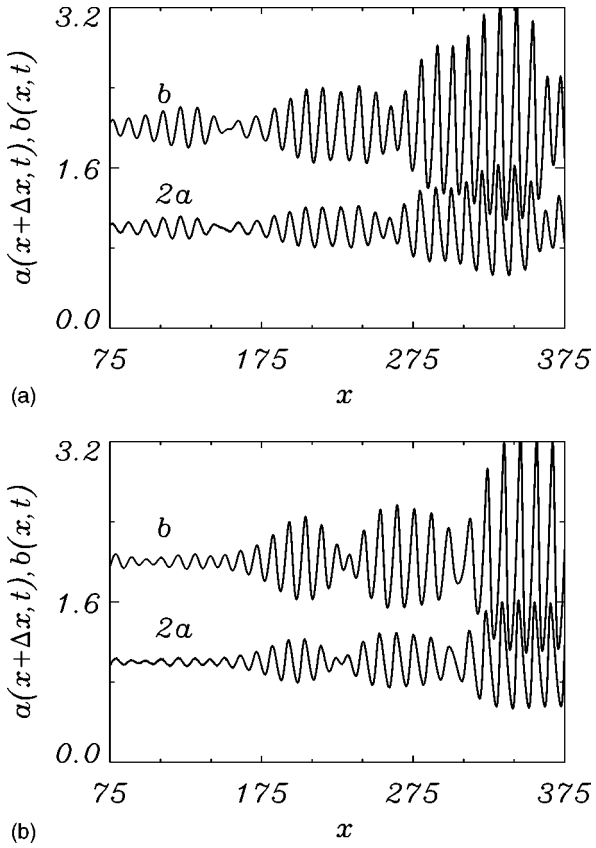

FIG. 5. Well developed NSSs for A and B as a function of x. Note the amplitude of the structures in comparison with Fig. 2. Parameters are $\mu=2.0$, $\phi=9.5$, $\epsilon=10^{-7}$, and (a) $t=460$ and (b) $t=528$. The value of Δx is the same as in Fig. 2.

for $\mu\to 1^+$ $(q_c\to 0)$, in the following section we show that, even in this limit case, a finite CCL can be defined.

IV. NOISE-SUSTAINED CROSS-CORRELATED STRUCTURES

In this section we give a numerical description [31] and a theoretical analysis of the NSSs observed in one and two spatial dimensions. We consider both cases separately.

A. One-dimensional case

For 1D systems the instability takes place at $q_x=\pm q_c$, and the noise keeps excited both wave vectors. To illustrate the dynamical evolution, in Figs. 5(a) and 5(b) we show snapshots of well developed noise-sustained patterns at two different times. We can appreciate that A and B support nonlocally cross-correlated NSSs, as was discussed in Sec. III [see Fig. 3(b)]. In fact, the patterns are not stationary, but drift in the direction of the flow. Although the structures travel to the right, they are continuously regenerated by dynamical amplification of noise that excites all the unstable modes at each space point—locally sustained. Thus, the general picture is that there is a competition between convectively unstable modes, which generates a nonlocally cross-correlated NSS for A and B, respectively. In Fig. 3(b) we can observe that the correlation reaches the order of the unity for

short times and the dynamics preserves the order of the correlation during time evolution.

Close to criticality, we numerically observe that the CCL does not change with respect to the value observed for short times. For example, the value of Δx is the same for Figs. 2, 5(a), and 5(b) ($\Delta x_{observed}=3.6\pm0.1$), in agreement with the obtained value from Eq. (11) ($\Delta x_{predicted}=3.69$). This fact can be explained in terms of a weakly nonlinear analysis. Near the critical point, a convective complex Ginzburg-Landau equation can be derived for a slowly varying envelope amplitude $\Psi(s,\tau)$ which governs the dynamics:

$$\begin{pmatrix} a \\ b \end{pmatrix}_{(x,s,t,\tau)} = \begin{pmatrix} a_0 \\ b_0 \end{pmatrix} + \epsilon\Psi(s,\tau)\Lambda(q_c,x)\exp(i\Omega_c t) + cc, \tag{12}$$

where $\tau=\epsilon^2 t$ (long time scale), $s=\epsilon x$ (long length scale), and $\epsilon=\sqrt{\phi-\phi_c}$ measures the distance to criticality. Equation (12) is valid to $O(\epsilon)$ (see Ref. [17] for derivation). The envelope $\Psi(s,\tau)$ governs the dynamics close to the instability threshold. However, as results from Eq. (12), the CCL is determined by the critical modes in a similar way that Eq. (9) determines Δx for the linearized dynamics.

The degree of correlation between species A and B depends on the noise intensity and/or distance to the threshold. For larger noise intensity and/or advection, the magnitude of the correlation is decreased but it keeps the order of magnitude for a wide range of values of the parameters. Actually, the same scenario is also observed in the presence of two independent sources of additive noise [one for each rate equation in Eqs. (2)], reflecting the fact that the noise(s) sustains the structures by driving the convectively unstable modes, which determines the CCL both in the linear and in the nonlinear regime.

A limiting situation is given when $\pm q_c$ collapses to zero. This occurs for $\mu\to1^+$; in this case $\phi_c\to0$ and for any finite value of ϕ there is a band of unstable modes with a large excited wave length. In the presence of a source of noise, the nonlinear wave number selection can be traced back to the behavior of the growth rate. At $\mu=1$ the instability takes place at $q=0$, but the most unstable modes have a non-null wave vector for $\phi>\phi_c$. To illustrate this fact, in Fig. 6(a) we show the growth rate of the unstable modes as a function of q for $\phi=0$—criticality—and for a non-null value of ϕ. Numerical simulations for $\mu=1$ indicate that NSSs with a finite CCL are solutions of Eq. (2) [see Fig. 6(b)]. As a result of the Fourier analysis, NSSs are generated by the unstable modes with maximum growth rate. Therefore, an estimation of Δx for $\mu=1$ can be obtained from this active unstable mode. For example, for the patterns of Fig. 6(b) the observed and predicted values for the CCL are $\Delta x=54.2\pm0.1$ and 58.69, respectively.

B. Two-dimensional case

For 2D chemical reactors the convective instability takes place at $q_y=0$, and the growth rate of the most unstable modes is maximum at $\vec{q}_c=(\pm q_c,0)$. For $\phi>\phi_c$, the $\vec{q}$ modes that satisfy $|q_x|\sim q_c$ and $|q_y|\lesssim q_c\sqrt{2(\phi-\phi_c)/\phi_c}$ are excited in the neighborhood of the critical point. The noise and the nonlinear competition keep all these wave vectors excited for long time and the most rapidly spreading modes interfere generating stripes. To illustrate the dynamical evolution, we show in Fig. 7 snapshots of the pattern configuration near threshold at three different times. The resulting structure is similar to that observed in the 1D case, except the smooth variations of the fronts along the y direction produced by the unstable q_y modes (with large wavelength), which are driven by noise. At the left side of the pattern the generation from noise of small-amplitude structures can be appreciated. This is a typical feature of NSSs in two spatial

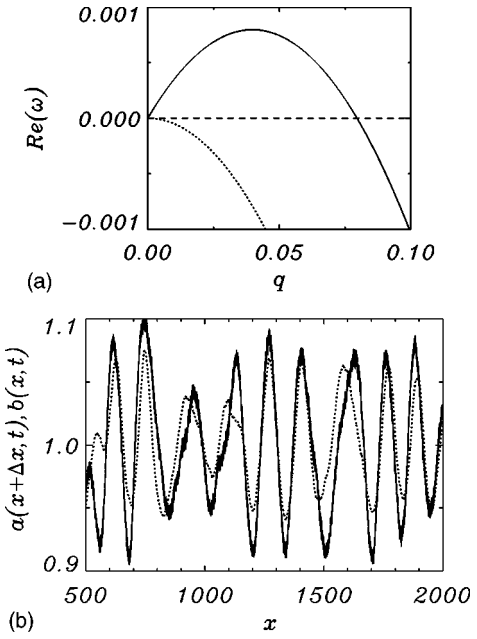

FIG. 6. (a) Real part of the eigenvalue ω as a function of q. The solid line corresponds to $\phi=0.08$ and the dotted line corresponds to criticality. Here $\mu=1$ ($\phi_c=0$). The most unstable modes correspond to the maximum of each line. (b) a and b as functions of x. Parameter values are $\mu=1$, $\phi=0.08$, $t=4491$, and $\epsilon=10^{-7}$. Here $\Delta x=54.2\pm0.1$ (note the x scale).

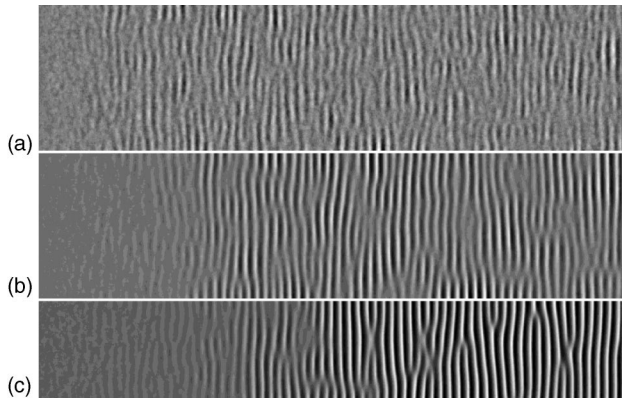

FIG. 7. Snapshots of $b(x,y,t)$ spontaneously generated from random initial conditions close to the trivial steady state: (a) $t=36$, (b) $t=68$, and (c) $t=272$. Parameters are $\mu=1.5$, $\phi=4.42$ ($\phi_c=3.87$), $\epsilon=0.0004$, $L_X=300$, and $L_Y=50$.

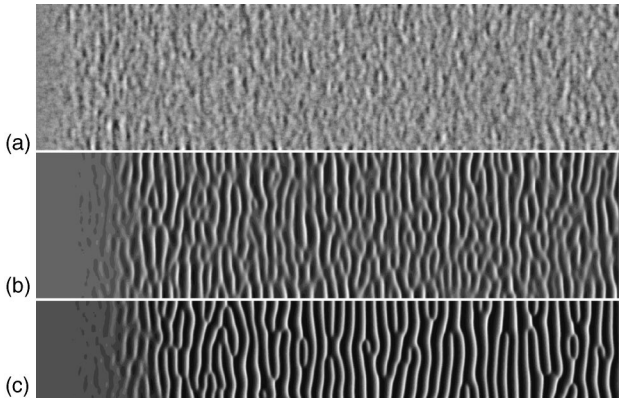

FIG. 8. Snapshots as in Fig. 7 for $\phi=10$; (a) $t=5$, (b) $t=15$, and (c) $t=45$. Parameters are $\mu=1.5$, $\epsilon=0.0006$, $L_X=750$, and $L_Y=125$.

dimensions [24,26]. We remark that the nonlocal cross correlation discussed previously for 1D systems is also observed near threshold in 2D structures. After transient, $b(x,y,t)$ becomes nonlocally cross correlated with $a(x+\Delta x,y,t)$, where the CCL is still given by Eq. (11). The agreement between the predicted and observed values of the CCL is as good as in the 1D case. For example, the observed and predicted values of Δx for the structures of Fig. 7 are 4.0 ± 0.25 and 4.12, respectively.

Far from threshold, strong variations appear in the front structure, as result from the noise-assisted activation of q_y modes. In this case, bifurcations and joints of fronts are observed during the time evolution. To illustrate this fact, in Fig. 8 we show snapshots of configurations at different times.

V. CONCLUSION

In conclusion, we have shown that NSSs can be generated in differential-flow reactors with cubic autocatalytic kinetics. They appear spontaneously in both activator and inhibitor species when the advection is above the threshold value. These structures are the result of a selective noise amplification by the dynamics in several orders of magnitude leading to the formation of stochastic self-organized structures.

We have analyzed the formation of NSSs for one and two spatial dimensions. Special features appear, due to the nature of the convectively unstable modes. In particular, they give rise to a nonlocal cross correlation between the NSSs that are observed both in the linear (short time) and the nonlinear regimes. The analytic expression for the CCL was contrasted with numerical simulations in 1D and 2D near threshold, with a good agreement between the observed and predicted values. For $\mu\rightarrow 1^{+}$, the dynamics becomes more complicated because the active modes are not closed to the critical ones, and the instability takes place at $\phi_c=0$. However, an estimation of the order of magnitude of the CCL is possible even in this case. The selected unstable modes also originate the observed orientation of the 2D stripes. Near threshold, 2D NSSs appear as quasi-one-dimensional, reflecting the fact that only long y wavelength modes are excited from noise. Far from threshold, irregular noise-sustained fronts are observed with appreciable variations along the y axis, as a result of the noise activation of a larger number of q_y modes.

We finally point out that chemical NSSs should be observable for different chemical reactions in differential-flow reactors. The imposed flow breaks the spatial symmetry of the system for any reaction in a generic way, allowing eventual convective instabilities. Thus, we expect that chemical NSSs should be observed in differential-flow reactors under very general conditions; we hope that these results can be qualitatively applied to other autocatalytic chemical systems with the DIFICI mechanism.

ACKNOWLEDGMENT

We acknowledge financial support from the National University of Mar del Plata.

[1] M.C. Cross and P.C. Hohenberg, Rev. Mod. Phys. **65**, 851 (1993).

[2] H.S. Wio, *An Introduction to Stochastic Processes and Nonequilibrium Statistical Physics* (World Scientific, Singapore, 1994).

[3] D. Walgraef, *Spatio-Temporal Pattern Formation* (Springer-Verlag, New York, 1996).

[4] G. Nicolis and I. Prigogine, *Self-Organization in Nonequilibrium Systems* (Wiley, New York, 1976); P.C. Fife, *Mathematical Aspects of Reacting and Diffusing Systems*, Lecture Notes in Biomathematics, Vol. 28 (Springer, Berlin, 1979); in *Nonequilibrium Cooperative Phenomena in Physics and Related Fields*, edited by M.G. Velarde (Plenum, New York, 1984), p. 371; G. Nicolis, T. Erneux, and M. Herschkowitz-Kaufman, in *Advances in Chemical Physics*, edited by I. Prigogine and S. Rice (Wiley, New York, 1978), Vol. 38.

[5] D. Walgraef, G. Dewel, and P. Borckmans, Phys. Rev. A **21**, 397 (1980); Adv. Chem. Phys. **XLIX**, 311 (1982); Q. Ouyang and H.L. Swinney, Nature (London) **352**, 610 (1991); G. Dewel *et al.*, Physica A **213**, 181 (1995).

[6] E. Mielczarek, J. Turner, D. Leiter, and L. Davis, Am. J. Phys. **51**, 32 (1983).

[7] M. Orban, P. de Kepper, I.R. Epstein, and K. Kustin, Nature (London) **282**, 816 (1981); S. Jakubith, H.H. Rotermund, W. Engel, A. von Oertzen, and G. Ertl, Phys. Rev. Lett. **65**, 3013 (1990).

[8] Y. Kuramoto, *Chemical Oscillations, Waves and Turbulence* (Springer, Berlin, 1984).

[9] V. Castets, E. Dulos, J. Boissonade, and P. De Kepper, Phys. Rev. Lett. **64**, 2953 (1990).

[10] A. Turing, Philos. Trans. R. Soc. London, Ser. B **237**, 37 (1952).

[11] H. Meinhardt, *Models of Biological Pattern Formation* (Academic, New York, 1982).

[12] A.B. Rovinsky and M. Menzinger, Phys. Rev. Lett. **69**, 1193 (1992).

[13] A.B. Rovinsky and M. Menzinger, Phys. Rev. Lett. **70**, 778 (1993).
[14] V.Z. Yakhnin, A.B. Rovinsky, and M. Menzinger, Chem. Eng. Sci. **50**, 2853 (1995).
[15] X. Wu, S. Nakata, M. Menzinger, and A. Rovinsky, J. Phys. Chem. **100**, 15810 (1996).
[16] M. Sangalli, and H.C. Chang, Phys. Rev. E **49**, 5207 (1994).
[17] R.A. Satnoianu, J.H. Merkin, and S.K. Scott, Physica D **124**, 345 (1998).
[18] R.A. Satnoianu, J.H. Merkin, and S.K. Scott, Chem. Eng. Sci. **55**, 461 (2000).
[19] R.J. Deissler, Stat. Phys. **40**, 376 (1985); **54**, 1459 (1989); Physica D **56**, 303 (1992).
[20] I. Rehberg *et al.*, Phys. Rev. Lett. **67**, 596 (1991).
[21] K.L. Babcock, G. Ahlers, and D.S. Cannell, Phys. Rev. Lett. **67**, 3388 (1991).
[22] A. Tsameret and V. Steinberg, Phys. Rev. Lett. **67**, 3392 (1991).
[23] M. Santagiustina, P. Colet, M. San Miguel, and D. Walgraef, Phys. Rev. Lett. **79**, 3633 (1997).
[24] M. Santagiustina, P. Colet, M. San Miguel, and D. Walgraef, Phys. Rev. E **58**, 3843 (1998).
[25] L. Yang, Z. Hou, and H. Xin, J. Chem. Phys. **110**, 3591 (1999); **110**, 3591 (1999).
[26] G. Izús, M. Santagiustina, M. San Miguel, and P. Colet, J. Opt. Soc. Am. B **16**, 1592 (1999).
[27] G. Izús, M. Santagiustina, M. San Miguel, and P. Colet (unpublished).
[28] H. Ward, M.N. Ouarzazi, M. Taki, and P. Glorieux, Phys. Rev. E **63**, 016604 (2001).
[29] M. San Miguel and R. Toral, in *Instabilities and Nonequilibrium Structures VI*, edited by E. Tirapegui (Kluwer Academic, Dordrecht, 1998).
[30] J. García-Ojalvo, and J.M. Sancho, *Noise in Spatially Extended Systems* (Springer-Verlag, New York, 1999).
[31] Equations (2) have been integrated using a finite difference scheme. We use a grid of 8000 samples with a grid space $\Delta_x = 0.1$ and time step $\Delta_t = 0.0001$ in the 1D case (for $\mu = 1$ we use a grid of 24 000 samples); and we use a grid of 1000 $\times 250$ samples with $\Delta_{x,y} = 0.5$ and time step $\Delta_t = 0.0002$ in the 2D case.